Merging the Minnaert-k parameter with spectral unmixing to map forest heterogeneity with CHRIS/PROBA data

Verrelst, J ; Clevers, J G P W ; Schaepman, Michael E

DOI: https://doi.org/10.1109/TGRS.2010.2047400

Merging the Minnaert-k Parameter With Spectral Unmixing to Map Forest Heterogeneity With CHRIS/PROBA Data

Jochem Verrelst, Jan G. P. W. Clevers, and Michael E. Schaepman, *Senior Member, IEEE*

***Abstract*—The Compact High Resolution Imaging Spectrometer (CHRIS) mounted onboard the Project for Onboard Autonomy (PROBA) spacecraft is capable of sampling reflected radiation at five viewing angles over the visible and near-infrared regions of the solar spectrum with high spatial resolution. We combined the spectral domain with the angular domain of CHRIS data in order to map the surface heterogeneity of an Alpine coniferous forest during winter. In the spectral domain, linear spectral unmixing of the nadir image resulted in a canopy cover map. In the angular domain, pixelwise inversion of the Rahman-Pinty-Verstraete (RPV) model at a single wavelength at the red edge (722 nm) yielded a map of the Minnaert-k parameter that provided information on surface heterogeneity at a subpixel scale. However, the interpretation of the Minnaert-k parameter is not always straightforward because fully vegetated targets typically produce the same type of reflectance anisotropy as non-vegetated targets. Merging both maps resulted in a forest cover heterogeneity map, which contains more detailed information on canopy heterogeneity at the CHRIS subpixel scale than is possible to realize from a single-source optical data set.**

***Index Terms*—Compact High Resolution Imaging Spectrometer (CHRIS), forest heterogeneity mapping, imaging spectroscopy, multi-angular, reflectance anisotropy.**

I. Introduction

THE MEASURED reflected solar radiation of boreal and Alpine forests under winter conditions depends on the wavelength and the proportions of snow cover and plant canopy cover detected by a sensor [1]. These proportions depend on illumination and viewing angle, topography, and structural canopy properties such as tree density, canopy geometry, and gap fraction. Consequently, the reflected radiation can be sampled by a space-borne optical sensor either in the spectral domain (i.e., at multiple wavelengths) in the angular domain (i.e., at various viewing angles) or as a combination of both. Though the inferring of information on the terrestrial surface from reflectance data sampled in the spectral domain has been extensively studied in the last 40 years (through image classification [2], [3], spectral vegetation indices [4], [5], surface reflectance models [6], [7], or spectral mixture analysis [8]), considerably less research has been done on exploiting reflectance data sampled in the angular domain for mapping applications [9]–[11].

With the advent of multi-angular earth observing sensors [12], [13] and the development of surface reflectance models [6], [7], physically-based attempts were undertaken to retrieve canopy characteristics from multi-angular reflectance data. Among the surface reflectance models, the Rahman-Pinty-Verstraete (RPV) parametric model [14] is particularly suitable for estimating reflectance anisotropy because it simulates the bidirectional reflectance distribution function (BRDF) of an arbitrary land surface on the basis of three parameters. Of these parameters, the k parameter is of particular interest as it describes most of the angular variation related to surface reflectance anisotropy [15]. Pinty *et al.* [15] theoretically demonstrated that the Minnaert-k parameter contains information on subpixel heterogeneity, particularly when a low solar zenith angle is present in combination with a bright background. Their work has been corroborated by other studies, e.g., on forest areas underlain by a snowpack [16]–[18].

In 2001 the European Space Agency (ESA) launched the experimental satellite sensor Compact High Resolution Imaging Spectrometer (CHRIS) onboard the Project for On-board Autonomy (PROBA) spacecraft. The imaging spectrometer captures quasi-instantaneously a series of five angular images of a terrestrial surface at a high spatial resolution ($\sim$17 m) during the same orbit. CHRIS is capable of sampling the anisotropic behavior of the reflected solar radiation in up to 62 narrow spectral bands over the visible and near-infrared (VNIR) regions of the electromagnetic spectrum (400–1050 nm) [13], [19].

To ascertain the capability of CHRIS for measuring reflectance anisotropy in the VNIR, an old-growth alpine forest stand in the Swiss Alps was chosen as a test site [20]. It was overflown by CHRIS-PROBA on March 17, 2007. On this day, the snow had melted from the tree canopy but the forest floor was still covered by a thick pack of snow, which spectrally simplified the image: dark overstory vegetation underlain by a bright snow-covered background. The concurrent spectrodirectional (combined spectral and multi-angular) observations of a

Manuscript received December 21, 2009; revised February 16, 2010. Date of publication May 18, 2010; date of current version October 27, 2010. This work was supported through the Dutch SRON GO program (Grant-No. EO-080). CHRIS/PROBA data were acquired under ESA AO proposal No. 2819 (Swiss National Park).

J. Verrelst was with the Centre for Geo-Information, Wageningen University, 6708 PB Wageningen, The Netherlands He is now with the Image Processing Laboratory, Valencia University, 46010 Valencia, Spain (e-mail: jochem.verrelst@wur.nl; jochem.verrelst@uv.es).

J. G. P. W. Clevers is with the Centre for Geo-Information, Wageningen University, 6708 PB Wageningen, The Netherlands (e-mail: jan.clevers@wur.nl).

M. E. Schaepman is with Remote Sensing Laboratories, University of Zurich, 8057 Zurich, Switzerland (e-mail: Michael.schaepman@geo.uzh.ch).

Color versions of one or more of the figures in this paper are available online at http://ieeexplore.ieee.org.

Digital Object Identifier 10.1109/TGRS.2010.2047400

spectrally simplified landscape at a high spatial and spectral resolution makes it possible to explore the spatial, spectral, and angular information content of spectrodirectional measurements to the fullest.

In the spectral domain, a widely applied technique is linear spectral unmixing [8]. It works particularly well in discriminating vegetation from snow cover, thereby generating a canopy cover map [18]. Canopy cover is defined as the percentage (from 0–100%) of a grid cell that is covered by a vegetation canopy. Linear unmixing techniques, however, are unable to provide information on the vertical distribution of canopy cover. Thus, linear unmixing techinques cannot reveal whether the canopy cover is of tall trees or short vegetation.

In the angular domain, a simple technique for obtaining information on surface reflectance anisotropy is the retrieval of the Minnaert-k parameter from the RPV model. Although the Minnaert-k parameter makes it possible to map variations in subpixel heterogeneity, the interpretation of the parameter is limited by various factors such as the parameter's dependence on solar zenith angle, background brightness, and topography [15], [17]. Further, the practical applicability of the Minnaert-k parameter is not always straightforward. Surfaces that behave radiatively like turbid media (typically, they are homogeneous surfaces that are either fully vegetated or non-vegetated) result in a bowl-shaped reflectance anisotropy pattern [15], and thus cannot be directly discriminated from each other. A possible way to overcome this and to improve forest heterogeneity mapping is to merge Minnaert-k information with the information content obtained from the spectral domain. The two aims of the study we describe here were therefore 1) to merge the Minnaert-k map with a spectrally-derived canopy cover map and 2) to ascertain whether the resulting map contains more valuable information related to canopy structure at the CHRIS subpixel scale than the single-source maps.

II. Biophysical Interpretation of Minnaert-k

The RPV model provides a description of the target's reflectance anisotropy without attempting to assign it to specific physical causes or processes. As such, it is an empirical and efficient parametric representation of that surface property [14], [15]. The RPV model splits the scattered radiation field for a given wavelength into a scalar amplitude component and an associated directional component describing the anisotropy of the surface [14], [15]. The directional component of the reflectance function is expressed as the product of three functions: 1) the modified Minnaert function k that controls the curvature (e.g., the degree of convexity or concavity), 2) a parameter that controls the degree of forward and backward scattering regimes; and 3) an optional hotspot descriptor function. The underlying algorithms for each of the parameters are documented in [14], [15].

Under favorable conditions of illumination and background brightness, the angular pattern is largely controlled by the physical properties and geometrical arrangements of the plant elements that constitute the terrestrial surfaces [15]. This means that the angular signature of a pixel at a single wavelength as measured by a multi-angular sensor can be diagnostic for the assessment of subpixel structural surface properties when there is sufficient difference in brightness between the overstory and background.

Coniferous forests commonly appear darker than deciduous forests due to the strong internal shadowing caused by clumping effects and the relatively high light absorption capacity of needle foliage [21]. In coniferous stands in winter, the following situations can occur: a surface that is brighter at large oblique viewing angles in forward and backward scattering directions leads to a "bowl-shaped" reflectance anisotropy pattern. A bowl-shaped anisotropy pattern results in a k value smaller than 1. This is a common situation for more homogeneous surface covers. Conversely, a surface that is brighter at nadir viewing angle than at oblique viewing angles leads to the inverse pattern: a "bell-shaped" reflectance anisotropy pattern. A bell-shaped anisotropy pattern results in a k value larger than 1. This is a common situation for open, vertically elongated canopies with a bright background. Finally, a surface that exhibits Lambertian reflectance, i.e., the amount of scattered radiation is the same in all directions, results in a k value of 1 [15].

The Minnaert-k parameter can thus be used as a bioindicator for canopy heterogeneity simply on the basis of canopy closure and fluctuations in the amount of scattering and absorbing material at one specific wavelength [15], [16], [18], and [22]. While k values in excess of 1 are generated by targets that exhibit vertical structures and 3-D effects, k values less than 1 are typically associated with targets that behave radiatively like turbid media. As a result, the k parameter is of limited use for discriminating homogeneous surface covers (e.g., it may characterize either very sparse or very dense canopy covers).

To overcome this limitation and to improve subpixel heterogeneity mapping, we proposed to combine the Minnaert-k parameter to canopy cover derived from the spectral domain. Kayitakire & Defourny [23] concluded that in forested landscapes, the horizontal arrangement of the trees and the stand density influence the angular component of the reflectance more than tree height and diameter. The contribution of the background brightness is another crucial factor in governing the shape of reflectance anisotropy [15]. It therefore seems logical to derive a canopy cover map and combine that with the Minnaert-k map. Since illuminated snow and conifer tree crowns are spectrally highly separable, we used linear spectral unmixing (LSU) of the spectral dimension of the nadir CHRIS data for this purpose.

III. Methodology

A. Test Site and CHRIS Data

An Alpine valley, the Ofenpass valley, located in the Swiss National Park, South East Switzerland ($10°13'48''$E/$46°39'45''$N), was chosen as test site. The valley is characterized by a coniferous old-growth forest and patches of Alpine meadow. The forest can be classified as woodland associations of the *Erico-Pinetum mugo* type typified by relatively open and discontinuous stands. The forests vary in topography, openness, tree clumping, leaf area index (LAI), and woodiness. The

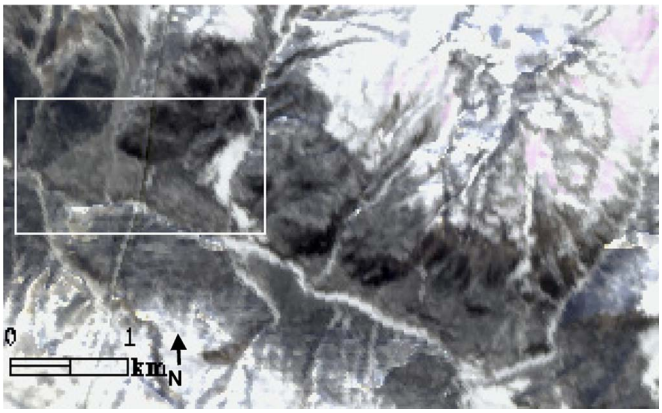

Fig. 1. Subset of the geometrically and atmospherically corrected CHRIS nadir scene acquired over the Swiss National Park study site on March 17, 2007. The Ofenpass valley stretches from top left to bottom right of the image. The whitish parts are snow-covered meadow fields or mountaintops. The square marks the core test site.

south-facing valley floor of the Ofenpass valley was considered to be the core test site (Fig. 1).

A series of CHRIS mode 5 "land" images was acquired over the Swiss National Park on March 17, 2007, near noon local time (11:34h local time; sun zenith: 50°, azimuth: 161°) under cloud-free conditions. Mode 5 is configured in CHRIS's best spatial resolution (nominally ~ 17 m) and spectral resolution (37 narrow bands with bandwidths of 6–33 nm located between 438 nm and 1036 nm). The acquisition date was chosen to ensure that a carpet of snow was still present while the sun position was already acceptably high at noon for the purpose of Minnaert-k retrievals. The solar position can be regarded as constant for all five CHRIS Fly-by Zenith Angles (FZA) since the images are instantly recorded during the satellite overpass. In the current along-track pointing configuration, the FZA is equivalent to the nominal viewing angles (0°, ±36°, ±55°). Due to its narrow field of view (FOV), however, CHRIS is only occasionally able to acquire a target at nominal viewing angle. PROBA must be tilted so that the target area falls within the sensor FOV. This means that the actual observation angles at which the images are acquired may deviate from the nominal viewing angles. For example, the nominal nadir camera position appeared to be pointing in a forward view zenith angle of $+21°$. A subset of the near-nadir image of the Ofenpass valley overpass is depicted in Fig. 1. The dark areas in the figure are the forest vegetation; the white patch within the dark forest represents a snow-covered meadow. Snow on the branches of the trees had melted, so in this case, "snow-covered forest" refers to snow covering the ground but not the trees.

Unfortunately the backward-pointing $-55°$ view zenith angle just missed the test site. The angular CHRIS scenes of the remaining four images were geometrically corrected following an approach for rugged, mountainous terrain [24] and were subsequently atmospherically corrected using a freely available MODTRAN-based procedure implemented in the BEAM toolbox (http://www.brockmann-consult.de/beam) that has been specifically developed for correcting CHRIS-PROBA images [25]. The end-to-end module simultaneously derives a set of calibration coefficients and an estimation of water vapor content and aerosol optical thickness from the data themselves. The preprocessing efforts resulted in geometrically corrected images of hemispherical directional reflectance factor (HDRF, see [26] for terminology used) data at a spatial resolution of 18 m. We did not include the bands in the blue part of the spectrum (442 and 489 nm) in our analysis because of the significant atmospheric scattering in the blue bands of CHRIS [27]. The bands close to the atmospheric water vapor absorption band at 940 nm (CHRIS bands at 925, 940 and 955 nm) were also omitted from further analysis.

B. Spectral and Angular Information

In the spectral domain, the reflectance of a pixel can be described by a spectral mixture model in which a mixed spectrum is represented as a linear combination of pure vegetation and snow spectra

$$R_i = \mathrm{f}_{\mathrm{vegetation}} R_{i,vegetation} + \mathrm{f}_{\mathrm{snow}} R_{i,snow} + \varepsilon_i \quad (1)$$

$$\text{under the constraint } \mathrm{f}_{\mathrm{vegetation}} + \mathrm{f}_{\mathrm{snow}} = 1 \quad \text{and } \mathrm{f} > 0 \quad (2)$$

where $\mathrm{f}_{\mathrm{vegetation}}$ and $\mathrm{f}_{\mathrm{snow}}$ are the fractions of vegetation and snow in the pixel studied, R_i is the reflectance of a pixel in band i, $R_{i,\mathrm{vegetation}}$ ($R_{i,\mathrm{snow}}$) is the reflectance of the vegetation (snow) endmember in band i, and ε_i is the residual error associated with band i. The full spectral domain (excluding the bands we had removed) was used to decompose the near-nadir image into fractions of these two endmembers. Hence, the LSU quantified the subpixel spectral contributions of canopy and underlying snow solely on the basis of mono-angular, near-nadir spectral measurements. The unmixing approach for the forest site was accompanied by uncertainty, expressed by the root mean square error (RMSE). Due to the spectrally simplified landscape, the RMSE values were consistently low (around 0.016). The results of the unmixing were compared with ground reference data collected following the VALERI protocol during the Fire Spread and Mitigation (SPREAD) campaign [28], [29]. Consistent results were obtained by LSU, though the canopy cover was systematically overestimated by about 8% by comparison with the ground reference data. The canopy cover map was subsequently stratified into canopy cover classes with increments of 10%, starting from 0% (full snow cover).

In the angular domain, reflectance anisotropy was quantified by means of the Minnaert-k parameter. Pixelwise retrieval of the Minnaert-k parameter through RPV model inversion was achieved using the RPVinversion-3 software package [30]. The inversion method is documented in [31]. The package offers a number of features, including the complete assessment of the measurement-model mismatch covariance matrix and the option of operating adjoint software codes derived from automatic differentiation techniques. This allowed us to perform the inversion of the nonlinear RPV model under the classical Bayesian approach in a numerically and computationally efficient manner while at the same time generating an unbiased estimation of the probability density functions for the parameters retrieved. The package implements the inverse model for two versions of the model, with or without the hotspot parameter. The hotspot parameter is only required to improve the representation of the

hotspot when illumination and observation geometries close to the hotspot are present. In the observed winter scene of CHRIS, this configuration was not of importance. The RPV inversion-3 package thus resulted in sets of RPV parameters and additional information on the accuracy of the fit expressed by the χ^2-statistic. Minnaert-k maps were generated on a pixel-by-pixel basis across all the used CHRIS wavelengths. Using canopy cover classes as a spatial mask, averaged Minnaert-k values were calculated per class across the CHRIS bands. This way, the Minnaert-k parameter can be systematically related to wavelength and canopy cover.

The Minnaert-k maps across the CHRIS bands and the canopy cover map were subsequently used to select the wavelength at which the best relationship between both data sources can be established. Given that low Minnaert-k values ($k < 1$) are expected at both very sparse and dense canopy covers (homogeneous surface covers) and high values ($k > 1$) at medium dense covers (heterogeneous surface covers), we expected a quadratic trend. It has been demonstrated that given a bright background, a switch from bell to bowl shape is most likely to occur somewhere in the red edge [18]. CHRIS in mode 5, with its eight bands in the red edge, provides an excellent basis for selecting an appropriate wavelength. We based the selection of the wavelength, at which the best relationship between canopy cover map and Minnaert-k map occurred, on the Pearson's squared correlation coefficient of the quadratic-polynomial fit and an F-test to test the significance of the relationships.

The advantage of CHRIS is that its multidimensionality can be exploited to map forest cover heterogeneity at the CHRIS subpixel scale. Spectrodirectional CHRIS data are particularly useful for generating two kinds of maps: in the angular domain, the data allow Minnaert-k retrieval to be applied for a given wavelength by inverting the RPV model, whereas in the spectral domain, the data allow LSU to be applied for a given viewing angle. We then merged both independently-derived maps, $(\mathrm{LSU}_{\mathrm{RGB}} + \mathrm{Minnaert\_}k_{\mathrm{RGB}})/2$, to create a new data layer. In addition, the original horizontal and vertical color bars associated with the canopy cover and Minnaert-k maps were likewise converted to an RGB representation and merged to a 2-D legend with canopy cover in the x-direction and Minnaert-k in the y-direction [cf. Fig. 8(b)].

IV. Results and Discussion

A. Linear Umixing

The canopy cover map generated from the nadir spectral domain is displayed in Fig. 2. Its frequency distribution is displayed in Fig. 3. The white spot on the right represents a snow-covered meadow. The histogram shows that only a few pixels with low densities ($< 40\%$) were present, usually at the edge of the meadow and as gaps within the forest. The histogram also indicates that the canopy cover in most of the pixels is between 60 and 90%, which is typical for an Alpine forest stand (see Fig. 3). About 14% of the pixels represent other situations: a snow-covered meadow (middle right), riverbeds (striped patterns), and gaps within the forest. However, whereas the canopy cover map shows spatial variations in proportion of tree cover, the map is unable to indicate surface heterogeneity at subpixel level.

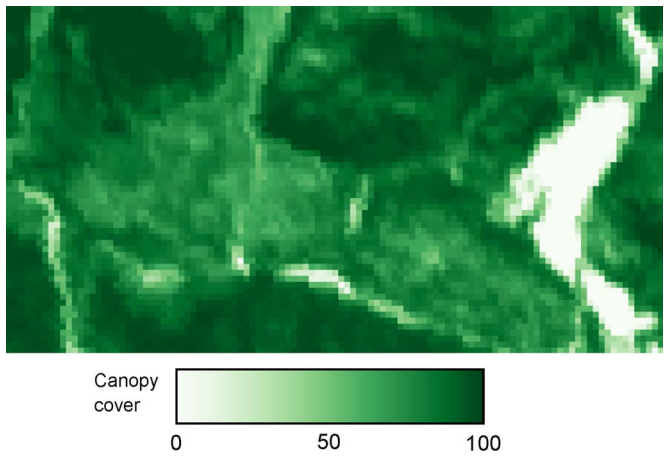

Fig. 2. Map of canopy cover based on constrained LSU of the nadir CHRIS image of March 17, 2007.

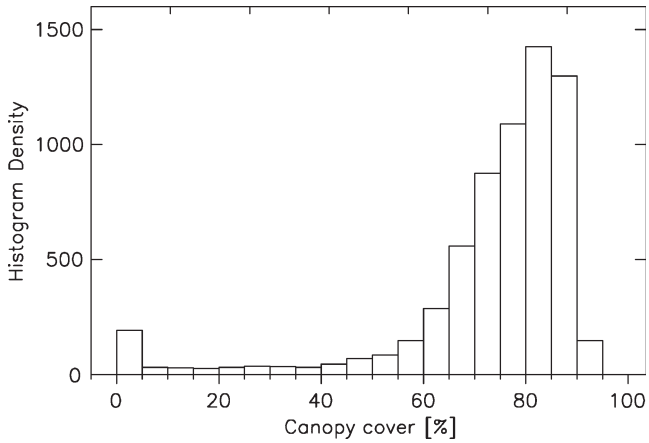

Fig. 3. Histogram of the canopy cover map based on constrained LSU of the nadir CHRIS data.

B. Minnaert-k Retrieval

Pixelwise inversion of the RPV model generated maps of Minnaert-k values across the CHRIS bands. In an earlier paper [18], we demonstrated some relationships between Minnaert-k, wavelength and canopy cover for the forest stands for a limited number of pixels on the valley floor (slope $< 7^\circ$). These relationships were again tested, but now for the whole region (Fig. 4). This figure shows a systematic, gridded overview of averaged Minnaert-k values for the wavelengths recorded by CHRIS along the x-axis and the canopy cover classes along the y-axis. This overview enables us to track the specific spectral trajectory of the Minnaert-k parameter for each canopy cover class.

Although the Minnaert-k parameter is a semi-empirical parameter, Fig. 4 shows that the bell-shaped and bowl-shaped reflectance anisotropies depend on both canopy cover and wavelength. For instance, the bell-shaped domain dominates throughout the visible region and narrows down to medium canopy cover densities throughout the red edge and early

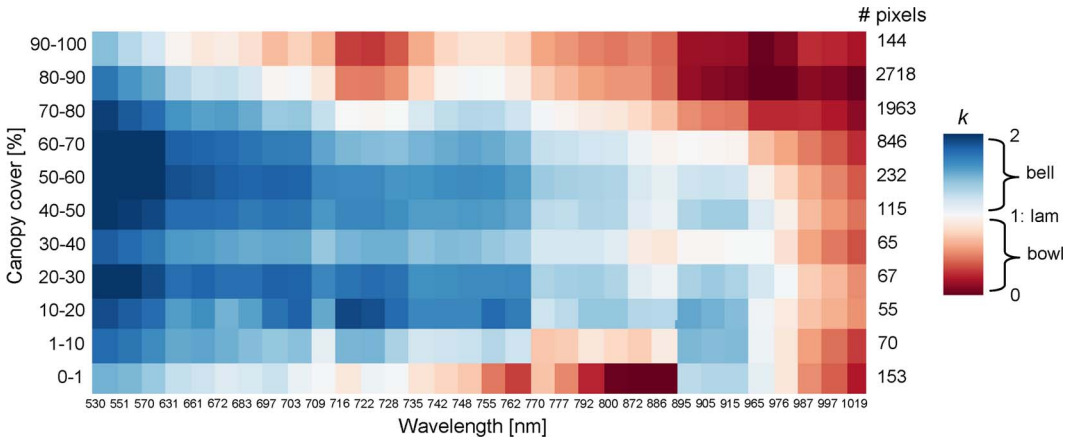

Fig. 4. Averaged Minnaert-k values as a function of canopy cover and wavelength. The numbers on the right represent the number of pixels for each class (lam = Lambertian).

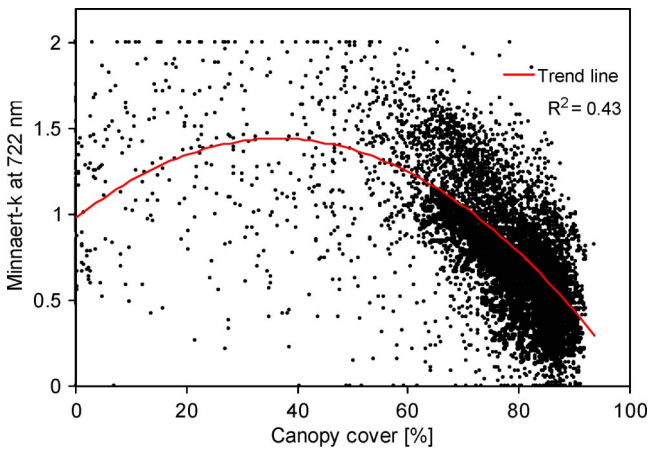

Fig. 5. Scatter plot of canopy cover against Minnaert-k at 722 nm. Trend line: $p < 0.0001$.

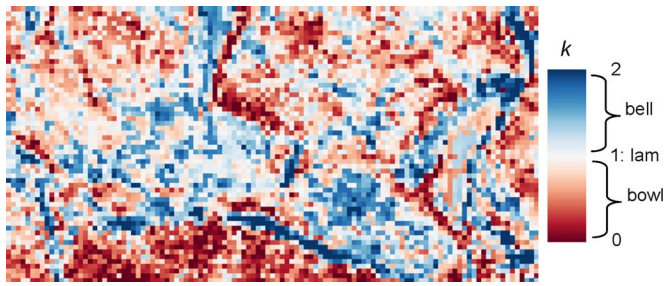

Fig. 6. Minnaert-k parameter obtained by RPV model inversion at 722 nm (lam = Lambertian).

NIR. Since reflectance anisotropy switches from bell-shape to bowl-shape in the red edge and early NIR as a function of canopy cover, it provides the critical spectral region for characterizing stand heterogeneity under winter conditions. The white color tones indicate the turning point from bell to bowl shape. See [18] for an exhaustive description of the underlying wavelength-dependent mechanisms related to land cover and sun-target-sensor geometry. The R^2 results of the quadratic regression model between canopy cover and Minnaert-k across the CHRIS bands for the complete data set yielded a best correlation at 722 nm (R^2 of 0.43). The relationship between the canopy cover map and the Minnaert-k map at 722 nm is shown in the scatter plot of Fig. 5. Although the relationship was significant $F_{2,6433} = 2405$, $p < 0.0001$), the low R^2 indicates that canopy cover is not the only variable determining reflectance anisotropy. This is particularly the case for pixels with canopy covers less than 60%, where no clear pattern can be observed. Most of these pixels with sparse forest cover are found at the interface between forest cover and snow-covered meadow or on riverbeds. At these locations, edge effects and the position of the edge in relation to the sun may yield varying anisotropy effects. Another explanation for the low R^2 is the influence of topographic effects. For pixels with $> 60\%$ canopy cover, the relationship between Minnaert-k and canopy cover is more obvious.

The Minnaert-k map at this wavelength is shown in Fig. 6. Whitish-blue color tones indicate the presence of a heterogeneous surface type such as open to medium dense forest stands with a cover density of up to 70%. Reddish-white color tones indicate the presence of a structurally homogeneous target such as a dense tree cover or a snow-covered meadow. Reddish-white patterns are to be found over the forest stands (e.g., the middle of the figure) but also over the snow-covered meadow (to the right). Such ambiguity of bowl-shaped patterns makes it hard to interpret this map for forest monitoring applications.

Although forest cover predominantly exhibited enhanced reflectance patterns in backscattering direction (with maximal backscatter at -36° zenith angle, which approaches closest the hot spot) and snow cover predominantly exhibited enhanced reflectance patterns in the forward scattering direction (due to its specular component), both land cover types yielded a bowl-shaped reflectance anisotropy pattern ($k < 1$). Therefore, from the generated Minnaert-k map, it is impossible to discern forest cover from non-forest cover. In addition, at a pixel size of 18 m, pixels with sparse forest cover at near-nadir may either lead to low k values (e.g., at the meadow) or high k values (e.g., at the riverbed). In the latter locations, reflectance anisotropy is strongly influenced by the volumetric contribution of the adjacent pixels (e.g., if adjacent pixels represent a dense forest cover, then lower reflectance values at larger viewing angles are observed due partly to pixel overlapping) in comparison to the near-nadir observation and so leading to a bell-shaped curvature

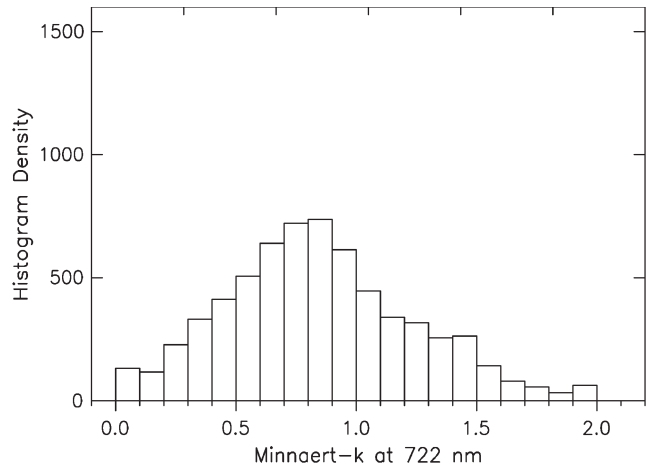

Fig. 7. Histogram of the Minnaert-k map inferred from the RPV model and angular CHRIS data at 722 nm.

(high k values). In case an irregular curvature is observed, the RPV inversion-3 package has been optimized to fit a smoother curvature in between the irregular values. The provided χ^2-statistics provide information how close the fit matches the observations of the four CHRIS viewing angles. At 722 nm 7.3% of the pixels led to a mismatch at a significance level of 0.05, mainly due to irregular reflectance anisotropy curvatures occurring on the meadow and riverbeds.

From Fig. 6, it is obvious that apart from vegetation structure, two spatial factors affect reflectance anisotropy at the CHRIS subpixel scale: 1) interfaces between land covers of contrasting volumetric compositions, e.g., forest-meadow interface, riverbeds, road intersections; and 2) topography variation in slope gradient and aspect, and the related variation in topographic shadowing. Both factors lead to the enhancement or attenuation of reflectance anisotropy patterns. The histogram related to the data in Fig. 6 has a normal distribution (Fig. 7), with a peak toward Minnaert-k values of 0.8 (small bowl-shaped pattern). Compared with the histogram of the canopy cover map (Fig. 3), the pattern is very different: the distribution has a wider spread, underlining that the spectral and angular domains are to a great extent independent of each other.

C. Merging

The merging of the canopy cover map with the Minnaert-k map is displayed in panel A of Fig. 8. In this merged map, not only is the snow-covered meadow (whitish color tones) clearly separated from the forest cover (greenish color tones), but subtle color tones related to subpixel heterogeneity also appear. The biophysical meaning of these color tones is explained in the 2-D color chart of panel B in Fig. 8.

In the 2-D color chart, all possible color tone combinations of Minnaert-k and canopy cover are displayed: canopy cover along the x-axis (generated from the spectral domain), Minnaert-k along the y-axis (generated from the angular domain). In the RGB color scheme, the green color represents the degree of canopy cover. The red color represents the degree of bowl-shaped reflectance anisotropy, whereas the blue color represents the degree of bell-shaped reflectance anisotropy. A pixel can either exhibit a degree of bowl-shape (red) or of bell-shape (blue). Briefly, the four corners of the 2-D color legend, representing the extreme situations that may theoretically occur, are:

1) *Pale blue color tones:* no canopy cover and maximal bell-shaped reflectance anisotropy. This is an unusual situation since subpixel heterogeneity is required to obtain a high Minnaert-k value, i.e., there must be some vegetation cover. However, some pixels at the meadow-forest interface approximate this situation due to the abrupt cessation of the vertically-elongated canopy. For instance, while from the nadir viewing angle on a meadow edge, no more forest cover is observed, it may happen that at a larger view zenith angle some contribution of adjacent forest cover is still observable.
2) *Dark bluish-green color tones:* maximal canopy cover and maximal bell-shaped reflectance anisotropy. This is also an unusual situation since a full cover behaves radiatively like turbid media, i.e., the canopy is so densely packed that no uncollided radiation exits the background snow cover to create a bell-shaped pattern. However, as soon as gaps appear in the cover (canopy cover $< 100\%$), bell-shaped patterns occur. This situation is observable for the pixels with the bluish-green color tones in Fig. 8 (panels A and C).
3) *Dark reddish-green color tones:* maximal canopy cover and maximal bowl-shaped anisotropy. This is a typical situation due to the homogeneous character of the dense canopy. Patches of dense forest cover are observable in Fig. 8 (panels A and C).
4) *Pale reddish color tones:* No canopy cover and maximal bowl-shaped anisotropy. This typically occurs on non-vegetated surfaces such as the snow-covered meadow.

As the canopy cover map solely provides fractions but no information about heterogeneity and the Minnaert-k map provides information on subpixel surface heterogeneity, the merged map provides information on both these attributes. The map shows that most of the pixels are situated between canopy covers of 60% and 90% and a Minnaert-k fluctuating between 0.3 and 1.5. Consequently, the pixels with bluish-green color tones refer to medium to dense forest cover with large subpixel heterogeneity ($k > 1$). See, for instance, region a in panel C of Fig. 8: here, more subtle variation in color tones is observable than in the canopy cover map of Fig. 2. The spatial pattern observed is thus not only due to the variation in canopy cover but also due to the variation in other parameters impacting reflectance anisotropy such as tree height. Although tree height may be a less influential factor than canopy cover [18], note that if the canopy cover consists of low-growing shrubs, then the variation in anisotropy would be smaller [17], [22], leading to paler bluish color tones. The pixels with dark bluish-green color tones typically represent areas with large, dark vertical structures (trees) in conjunction with open targets (i.e., gaps).

Conversely, the pixels with dark reddish-green color tones ($k < 1$) refer to dense forest covers that behave radiatively like turbid media and thus lack subpixel heterogeneity. That is, for instance, the case for region b in panel C of Fig. 8.

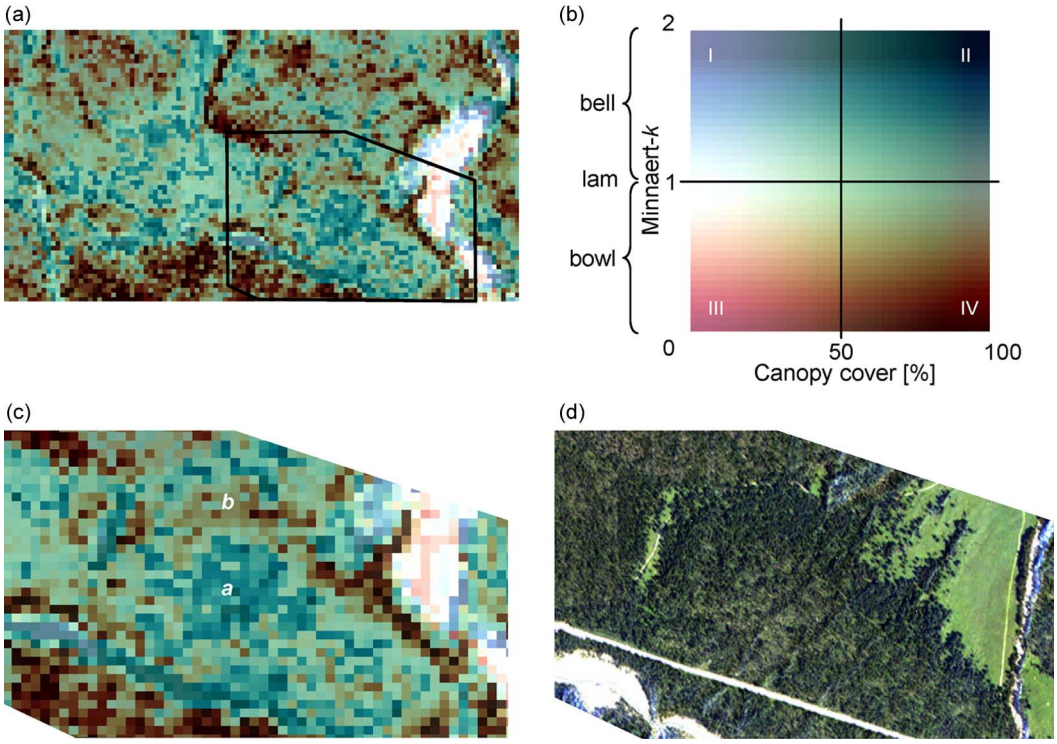

Fig. 8. (a) RGB result of merging the Minnaert-k map with the canopy cover map. (b) Two-dimensional color chart based on the color bar of the canopy cover map (x-axis) and the color bar of the Minnaert-k map (y-axis) (lam = Lambertian). (c) Zoom-in of the merged map as presented in panel A. (d) The reference image as derived from a high resolution stereo camera (HRSC) acquisition in summer 2003 (true color).

This region shows a canopy cover in which the canopy is so dense that it imposes a typical bowl-shaped anisotropy pattern. Tree height does not play a role here; the same type of bowl-shaped pattern occurs over homogeneous, flat targets (i.e., snow-covered meadow). Also of interest are the pale color tones ($k \approx 1$). These pixels represent surfaces that exhibit Lambertian reflectance without vegetation cover. They are to be found over the snow-covered meadow. Other snow-covered meadow pixels showed a typical bowl-shaped anisotropy behavior.

Our study has demonstrated that CHRIS data can be decomposed into its spectral and angular components by using linear unmixing and by deriving the Minnaert-k parameter. Both maps are useful for describing forest structure but have their specific advantages and limitations due to their single-source nature. Merging them to produce a combined map leads to an improved characterization of forest heterogeneity at subpixel scale that can be used for monitoring forest development or for parameterizing canopy reflectance models, enabling proper retrieval of biophysical (e.g., biomass) or biochemical (e.g., chlorophyll content) parameters [32], [33].

When interpreting the merged map, it should be noted that solar zenith angle, background brightness, and the position of the angular sampling in relation to the principal plane also exert influence on the spectrodirectional response. In addition, variations in topography and the spectral and anisotropy characteristics of land cover features other than snow and vegetation cover (e.g., sharp land cover edges, rock outcrops, water bodies) may affect the spectrodirectional response and, thus, the results of the merged map as well. These site-specific influences are nevertheless strongly related to pixel size. At a relatively high spatial resolution of 18 m and at trees that may reach up to 18 m, scattered radiation is influenced not only by variation in the horizontal plane (e.g., tree density) but also by variation in the vertical plane (e.g., variation in tree height). This implies that the pixel's reflectance at such a high spatial resolution is considerably impacted by radiation fluxes in the horizontal plane [34]. This impact is typically observable for pixels located at the forest-meadow interfaces where the radiation fluxes shift from a volumetric medium (pixel size approximately equal to stand height) to a flat medium (pixel size largely exceeding stand height). For application purposes, it might be therefore advisable to validate the inversion performance, e.g., by analyzing the fit of the original CHRIS measurements with the RPV-reconstructed measurements [18], [30]. At coarser pixel size (e.g., MISR at 275 m in red), on the other hand, tree-level anisotropy effects and edge effects tend to be smoothed, yielding more accurate fits but less detailed maps [15]. Alternatively, the use of LiDAR data may be an option to validate the informative value of reflectance anisotropy (e.g., see [17]); however, note that apart from the structural configuration, the spectral influence of background has to be accounted for [35] as well.

Regardless of the aforementioned limitations, problems related to co-registration and spatial resampling are minimized and processing can be fast and quasi-automatic because the angular and spectral domain originated from the same data source (CHRIS). The RPV inversion-3 package retrieves Minnaert-k fast and can easily be automated [26]. Additionally, provided χ^2 uncertainty measures can filter out poorly inverted pixels, wavelength selection can be resolved on the basis of statistical or physical indicators. The automatic identification of endmembers still has to be resolved, but numerous methods

are available to do this automatically [36]–[38]. Once this has been addressed, mapping forest heterogeneity can be further automated by combining information from the spectral and angular domains. However, more research on the robustness of the method may be necessary. For instance, it remains to be seen how successfully forest cover heterogeneity can be mapped during summer conditions when the spectral contrast between canopy and background is reduced due to the green-up of the undergrowth.

V. Conclusion

The European Space Agency's small PROBA satellite carries the only imaging spectrometer in space (CHRIS) that provides multi-angular measurements of the reflected solar radiation from the earth's surface at a high spatial resolution. This paper has demonstrated that combining canopy cover information derived from the spectral domain at one single viewing angle (nadir) with heterogeneity information derived from the angular domain at one single wavelength in the red edge (722 nm) generates spatially explicit information about forest cover heterogeneity at the CHRIS subpixel scale. The generated map included information on surface heterogeneity that was much more detailed than the information that can be derived from single-source optical data sets.

Acknowledgment

The authors would like to thank L. Guanter for the assistance with the atmospheric preprocessing, and also J. Burrough for the advice on the English. The authors would like to thank the two anonymous reviewers for their valuable comments.

References

[1] D. Vikhamar and R. Solberg, "Subpixel mapping of snow cover in forests by optical remote sensing," *Remote Sens. Environ.*, vol. 84, no. 1, pp. 69–82, Jan. 2003.

[2] D. Lu and Q. Weng, "A survey of image classification methods and techniques for improving classification performance," *Int. J. Remote Sens.*, vol. 28, no. 5, pp. 823–870, Jan. 2007.

[3] J. Muñoz-Marí, L. Bruzzone, and G. Camps-Valls, "A support vector domain description approach to supervised classification of remote sensing images," *IEEE Trans. Geosci. Remote Sens.*, vol. 45, no. 8, pp. 2683–2692, Aug. 2007.

[4] E. P. Glenn, A. R. Huete, P. L. Nagler, and S. G. Nelson, "Relationship between remotely-sensed vegetation indices, canopy attributes and plant physiological processes: What vegetation indices can and cannot tell us about the landscape," *Sensors*, vol. 8, no. 4, pp. 2136–2160, Mar. 2008.

[5] D. Haboudane, N. Tremblay, J. R. Miller, and P. Vigneault, "Remote estimation of crop chlorophyll content using spectral indices derived from hyperspectral data," *IEEE Trans. Geosci. Remote Sens.*, vol. 46, no. 2, pp. 423–436, Feb. 2008.

[6] W. Verhoef, "Light scattering by leaf layers with application to canopy reflectance modeling: The SAIL model," *Remote Sens. Environ.*, vol. 16, no. 2, pp. 125–141, Oct. 1984.

[7] M. M. Verstraete, B. Pinty, and R. E. Dickinson, "A physical model of the bidirectional reflectance of vegetation canopies: 1. Theory," *J. Geophys. Res.*, vol. 95, no. D8, pp. 11 755–11 765, Jul. 1990.

[8] A. Plaza, P. Martínez, R. Pérez, and J. Plaza, "A quantitative and comparative analysis of endmember extraction algorithms from hyperspectral data," *IEEE Trans. Geosci. Remote Sens.*, vol. 42, no. 3, pp. 650–663, Mar. 2004.

[9] M. E. Schaepman, "Spectrodirectional remote sensing: From pixels to processes," *Int. J. Appl. Earth Obs. Geoinformation*, vol. 9, no. 2, pp. 204–223, May 2007.

[10] D. J. Diner, J. V. Martonchik, R. A. Kahn, B. Pinty, N. Gobron, D. L. Nelson, and B. N. Holben, "Using angular and spectral shape similarity constraints to improve MISR aerosol and surface retrievals over land," *Remote Sens. Environ.*, vol. 94, no. 2, pp. 155–171, Jan. 2005.

[11] M. Chopping, G. G. Moisen, L. Su, A. Laliberte, A. Rango, J. V. Martonchik, and D. P. C. Peters, "Large area mapping of southwestern forest crown cover, canopy height, and biomass using the NASA Multiangle Imaging Spectro-Radiometer," *Remote Sens. Environ.*, vol. 112, no. 5, pp. 2051–2063, May 2008.

[12] D. J. Diner, G. P. Asner, R. Davies, Y. Knyazikhin, C. B. Schaaf, J. P. Muller, A. W. Nolin, J. Stroeve, and B. Pinty, "New directions in Earth observing: Scientific applications of multiangle remote sensing," *Bull. Amer. Meteorol. Soc.*, vol. 80, no. 11, pp. 2209–2228, Nov. 1999.

[13] M. J. Barnsley, J. J. Settle, M. A. Cutter, D. R. Lobb, and F. Teston, "The PROBA/CHRIS mission: A low-cost smallsat for hyperspectral multiangle observations of the Earth surface and atmosphere," *IEEE Trans. Geosci. Remote Sens.*, vol. 42, no. 7, pp. 1512–1520, Jul. 2004.

[14] H. Rahman, M. M. Verstraete, and B. Pinty, "Coupled Surface-Atmosphere Reflectance (CSAR) Model .2. Semi-empirical surface model usable with NOAA Advanced Very High Resolution Radiometer data," *J. Geophys. Res.-Atmos.*, vol. 98, no. D11, pp. 20 791–20 801, Nov. 1993.

[15] B. Pinty, J. L. Widlowski, N. Gobron, M. M. Verstraete, and D. J. Diner, "Uniqueness of multiangular measurements—Part I: An indicator of subpixel surface heterogeneity from MISR," *IEEE Trans. Geosci. Remote Sens.*, vol. 40, no. 7, pp. 1560–1573, Jul. 2002.

[16] A. W. Nolin, "Towards retrieval of forest cover density over snow from the Multi-angle Imaging SpectroRadiometer (MISR)," *Hydrol. Process.*, vol. 18, no. 18, pp. 3623–3636, Dec. 2004.

[17] B. Koetz, M. Kneubühler, J. L. Widlowski, F. Morsdorf, M. Schaepman, and K. Itten, "Assessment of canopy structure and heterogeneity from multi-angular CHRIS-PROBA data," in *Proc. 9th SPMSRS*, Beijing, China, 2005, pp. 73–78.

[18] J. Verrelst, M. E. Schaepman, and J. G. P. W. Clevers, "Spectrodirectional Minnaert-*k* retrieval using CHRIS/PROBA data," in preparation.

[19] R. Duca and F. Del Frate, "Hyperspectral and multiangle CHRIS-PROBA images for the generation of land cover maps," *IEEE Trans. Geosci. Remote Sens.*, vol. 46, no. 10, pp. 2857–2866, Oct. 2008.

[20] M. E. Schaepman, B. Koetz, G. Schaepman-Strub, N. E. Zimmermann, and K. I. Itten, "Quantitative retrieval of biogeophysical characteristics using imaging spectroscopy—A mountain forest case study," *Community Ecology*, vol. 5, no. 1, pp. 93–104, Jun. 2004.

[21] S. Smolander and P. Stenberg, "A method to account for shoot scale clumping in coniferous canopy reflectance models," *Remote Sens. Environ.*, vol. 88, no. 4, pp. 363–373, Dec. 2003.

[22] J. L. Widlowski, B. Pinty, N. Gobron, M. M. Verstraete, D. J. Diner, and A. B. Davis, "Canopy structure parameters derived from multi-angular remote sensing data for terrestrial carbon studies," *Clim. Change*, vol. 67, no. 2/3, pp. 403–415, 2004.

[23] F. Kayitakire and P. Defourny, "Forest type discrimination using multi-angle hyperspectral data," in *Proc. 2nd CHRIS/PROBA Workshop, ESA SP*, Frascati, Italy, 2004, pp. 72–84.

[24] M. Kneubühler, B. Koetz, R. Richter, M. Schaepman, and K. Itten, "Geometric and radiometric pre-processing of CHRIS/PROBA data over mountainous terrain," in *Proc. 3rd CHRIS/PROBA Workshop, ESA SP*, 2005, pp. 59–64.

[25] L. Guanter, L. Alonso, and J. Moreno, "A method for the surface reflectance retrieval from PROBA/CHRIS data over land: Application to ESA SPARC campaigns," *IEEE Trans. Geosci. Remote Sens.*, vol. 43, no. 12, pp. 2908–2917, Dec. 2005.

[26] G. Schaepman-Strub, M. E. Schaepman, T. H. Painter, S. Dangel, and J. V. Martonchik, "Reflectance quantities in optical remote sensing—Definitions and case studies," *Remote Sens. Environ.*, vol. 103, no. 1, pp. 27–42, Jul. 2006.

[27] L. Guanter, L. Alonso, and J. Moreno, "Atmospheric corrections of CHRIS/PROBA data acquired in the SPARC campaign," in *Proc. 2nd CHRIS/PROBA Workshop*, Frascati, Italy, 2004.

[28] B. Kötz, M. Schaepman, F. Morsdorf, P. Bowyer, K. Itten, and B. Allgower, "Radiative transfer modeling within a heterogeneous canopy for estimation of forest fire fuel properties," *Remote Sens. Environ.*, vol. 92, no. 3, pp. 332–344, Aug. 2004.

[29] F. Morsdorf, E. Meier, B. Kötz, K. I. Itten, M. Dobbertin, and B. Allgöwer, "LIDAR-based geometric reconstruction of boreal type forest stands at single tree level for forest and wildland fire management," *Remote Sens. Environ.*, vol. 92, no. 3, pp. 353–362, Aug. 2004.

[30] T. Lavergne, T. Kaminski, B. Pinty, M. Taberner, N. Gobron, M. M. Verstraete, M. Vossbeck, J. L. Widlowski, and R. Giering, "Application to MISR land products of an RPV model inversion package using

adjoint and Hessian codes," *Remote Sens. Environ.*, vol. 107, no. 1/2, pp. 362–375, Mar. 2007.
[31] N. Gobron and D. Lajas, "A new inversion scheme for the RPV model," *Can. J. Remote Sens.*, vol. 28, no. 2, pp. 156–167, 2002.
[32] J. Verrelst, M. E. Schaepman, B. Koetz, and M. Kneubühler, "Angular sensitivity analysis of vegetation indices derived from CHRIS/PROBA data," *Remote Sens. Environ.*, vol. 112, no. 5, pp. 2341–2353, May 2008.
[33] L. Kooistra, W. Wamelink, G. Schaepman-Strub, M. Schaepman, H. van Dobben, U. Aduaka, and O. Batelaan, "Assessing and predicting biodiversity in a floodplain ecosystem: Assimilation of net primary production derived from imaging spectrometer data into a dynamic vegetation model," *Remote Sens. Environ.*, vol. 112, no. 5, pp. 2118–2130, May 2008.
[34] J. L. Widlowski, B. Pinty, T. Lavergne, M. M. Verstraete, and N. Gobron, "Horizontal radiation transport in 3-D forest canopies at multiple spatial resolutions: Simulated impact on canopy absorption," *Remote Sens. Environ.*, vol. 103, no. 4, pp. 379–397, Aug. 2006.
[35] J. Pisek, J. M. Chen, J. R. Miller, J. R. Freemantle, J. I. Peltoniemi, and A. Simic, "Mapping forest background reflectance in a boreal region using multiangle compact airborne spectrographic imager data," *IEEE Trans. Geosci. Remote Sens.*, vol. 48, no. 1, pp. 499–510, Jan. 2010.
[36] P. J. Martínez, R. M. Pérez, A. Plaza, P. L. Aguilar, M. C. Cantero, and J. Plaza, "Endmember extraction algorithms from hyperspectral images," *Ann. Geophys.*, vol. 49, no. 1, pp. 93–101, Feb. 2006.
[37] M. Zortea and A. Plaza, "Spatial preprocessing for endmember extraction," *IEEE Trans. Geosci. Remote Sens.*, vol. 47, no. 8, pp. 2679–2693, Aug. 2009.
[38] R. Zurita-Milla, J. G. P. W. Clevers, and M. E. Schaepman, "Unmixing-based landsat TM and MERIS FR data fusion," *IEEE Geosci. Remote Sens. Lett.*, vol. 5, no. 3, pp. 453–457, Jul. 2008.

Jochem Verrelst received the M.Sc. degree in tropical land use and geo-information science and the Ph.D. degree in remote sensing from Wageningen University, Wageningen, The Netherlands, in 2005 and 2010, respectively. The subject of his dissertation was on the space-borne spectrodirectional estimation of forest properties.

Since March 2010, he has been with the Image Processing Laboratory, University of Valencia, Valencia, Spain. His research interests include retrieval of vegetation properties using airborne and satellite data, canopy radiative transfer modeling, and multi-angular and hyperspectral data analysis.

Jan G. P. W. Clevers received the M.Sc. degree in agronomy and the Ph.D. degree in remote sensing from Wageningen University, Wageningen, The Netherlands, in 1981 and 1986, respectively. The subject of his dissertation was on the application of remote sensing to agricultural field trials and he developed a practical applicable reflectance model for estimating crop characteristics.

His present activities concern the continuation of the developments of optical reflectance models (including bidirectional reflectance and hyperspectral measurements), the linking to crop growth models, the synergy hypothesis with the purpose of the combined use of optical and microwave observations as well as of prior knowledge, and land cover mapping using remote sensing data at different scales. He has been a Project Manager of several projects within the Dutch National Remote Sensing Program and of a JRC study contract. He has contributed to more than 50 peer-reviewed journal papers. He is currently an Associate Professor and Lecturer in remote sensing at Wageningen University.

Michael E. Schaepman (M'05–SM'07) received the M.Sc. and Ph.D. degrees in geography from the University of Zurich (CH), Zurich, Switzerland, in 1993 and 1998, respectively.

In 1999, he spent his Postdoctoral time at the Optical Science Center, University of Arizona, Tucson. In 2000, he was appointed Project Manager of the ESA Airborne Prism Experiment (APEX) spectrometer. In 2003, he accepted a position as Full Chair of geo-information science and remote sensing at Wageningen University, Wageningen, The Netherlands. In 2009, he was appointed Full Chair of remote sensing at the University of Zurich (CH). He is currently heading the Remote Sensing Laboratories of this same university. His interests are in computational earth sciences using remote sensing and physical models, with particular focus on the land–atmosphere interface using imaging spectroscopy.